Biochemistry
Article
Cite This: Biochemistry 2018, 57, 1190−1200
pubs.acs.org/biochemistry

Stabilizing Leaf and Branch Compost Cutinase (LCC) with Glycosylation: Mechanism and Effect on PET Hydrolysis

Abhijit N. Shirke,[†,‡] Christine White,[§] Jacob A. Englaender,[∥] Allison Zwarycz,[∥] Glenn L. Butterfoss,[⊥] Robert J. Linhardt,[†,‡,§,∥] and Richard A. Gross*,[†,‡,§]

[†]Department of Chemistry and Chemiscal Biology, Rensselaer Polytechnic Institute, Troy, New York 12180, United States
[‡]Center for Biotechnology and Interdisciplinary Studies, Rensselaer Polytechnic Institute, Troy, New York 12180, United States
[§]Department of Chemical and Biological Engineering, Rensselaer Polytechnic Institute, Troy, New York 12180, United States
[∥]Department of Biology, Rensselaer Polytechnic Institute, Troy, New York 12180, United States
[⊥]Center for Genomics and Systems Biology, New York University Abu Dhabi, Abu Dhabi, UAE

Supporting Information

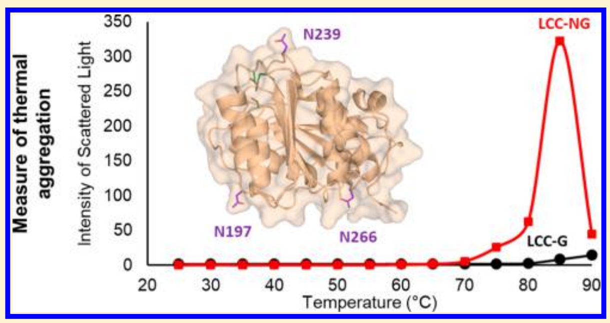

ABSTRACT: Cutinases are polyester hydrolases that show a remarkable capability to hydrolyze polyethylene terephthalate (PET) to its monomeric units. This revelation has stimulated research aimed at developing sustainable and green cutinase-catalyzed PET recycling methods. Leaf and branch compost cutinase (LCC) is particularly suited toward these ends given its relatively high PET hydrolysis activity and thermostability. Any practical enzymatic PET recycling application will require that the protein have kinetic stability at or above the PET glass transition temperature (T_g, i.e., 70 °C). This paper elucidates the thermodynamics and kinetics of LCC conformational and colloidal stability. Aggregation emerged as a major contributor that reduces LCC kinetic stability. In its native state, LCC is prone to aggregation owing to electrostatic interactions. Further, with increasing temperature, perturbation of LCC's tertiary structure and corresponding exposure of hydrophobic domains leads to rapid aggregation. Glycosylation was employed in an attempt to impede LCC aggregation. Owing to the presence of three putative N-glycosylation sites, expression of native LCC in *Pichia pastoris* resulted in the production of glycosylated LCC (LCC-G). LCC-G showed improved stability to native state aggregation while increasing the temperature for thermal induced aggregation by 10 °C. Furthermore, stabilization against thermal aggregation resulted in improved catalytic PET hydrolysis both at its optimum temperature and concentration.

Cutinase catalyzed hydrolysis of polyethylene terephthalate (PET) is a promising enzymatic route for green and sustainable recycling processes.[1−6] A commercially viable enzyme for PET recycling will require both high catalytic turnover and kinetic stability at temperatures above PET's glass transition (T_g, i.e., 70 °C), at which point chain mobility is increased in the amorphous phase allowing improved access to ester links between repeat units.[6,7] Among the several cutinases characterized for PET hydrolysis (e.g., *Fusarium solani* cutinase (FsC),[8] *Humicola insolens* cutinase (HiC),[6,9] *Thermobifida fusca* cutinase (TfC)[10]), Leaf and branch compost cutinase (LCC)[5,11] may be the most promising given that the wild-type already provides both high PET catalytic activity and thermostability. Recently, Yoshida et al. reported a comparative activity analysis of LCC, TfC and a newly identified enzyme PETase.[3] LCC outperformed both cutinases due in part to its structural stability at higher temperatures.[11] However, PETase was most active for PET hydrolysis at room temperature.[3]

Sulaiman et al. discovered LCC through a metagenomic screen of DNA from leaf and branch compost.[5] Although the native host of the enzyme is not known, it is of bacterial origin based on its significant sequence identity with several bacterial cutinases (e.g., 52% with *Thermobifida alba* cutinase, TbC;[11] 46% identity with *Thermobifida fusca* cutinase, TfC).[10] The authors subsequently reported LCC's crystal structure and characterized its structural stability and PET hydrolysis activity. LCC is highly thermostable with a T_m of 86 °C, which, in the presence of 20 mM $CaCl_2$, increases by an additional 12 °C.[11] This is the highest cutinase thermostability thus far reported.

Despite its high thermodynamic stability (T_m 86 °C), LCC displays a surprisingly low kinetic stability. Sulaiman and co-workers found the enzyme has half-lives of just 40 and 7 min at 70 and 80 °C, respectively.[5,11] However, the authors did not further investigate the gap between LCC thermodynamic and kinetic stability. This is a crucial problem that must be understood and rectified for practical applications such as PET recycling. With

Received: November 25, 2017
Revised: January 11, 2018
Published: January 12, 2018

DOI: 10.1021/acs.biochem.7b01189
Biochemistry 2018, 57, 1190−1200

this in mind, we conducted a preliminary thermal deactivation analysis revealing that LCC displays a high aggregation propensity, a primary contributor to its thermal deactivation.

Aggregation is a colloidal property arising when solute−solute (protein−protein) interactions are strong relative to solute−solvent (protein−solvent) interactions.[12,13] These interactions are generally dominated by electrostatic[14,15] or hydrophobic attractions.[16,17] Proteins in their native form often display a surface, which, at low concentration and ambient conditions (native conditions), has a low propensity for aggregation. However, higher protein concentrations (such as those used for storage) may promote aggregation and lead to formulation challenges.[18] Furthermore, harsh reaction conditions (e.g., pH, chemical, temperatures, agitation) can induce conformational and protonation changes leading to aggregation at lower concentrations.[19−23] Strategies to inhibit aggregation involve both colloidal and conformational stabilization of the protein. The most common solutions include: (i) protein engineering to improve conformational stability,[24] (ii) protein engineering to inhibit protein aggregation,[16,25,26] (iii) use of chemical additives,[27,28] and (iv) chemical modification of the protein (e.g., PEGylation, HESylation, etc.).[29−31] However, protein engineering may be time-consuming when a remedy to the problem is not obvious from modeling. Addition of chemical additives may be economically prohibitive. Finally, selective chemical modifications are often difficult and may lead to a distribution of protein populations with differing stability/activity.

Glycosylation site engineering can provide a practical solution against thermal aggregation. Glycosylation is a covalent attachment of an oligosaccharide to the protein carried out as a post-translational modification by eukaryotes.[32] Glycosylation can impede aggregation by improving protein conformational stability[33,34] or by imposing steric constraints that inhibit protein−protein interactions.[35−37] Stabilization by glycosylation will be a function of the number of glycosylation sites and their location(s).[33,38,39] There are two primary classes of natural glycosylation: (1) O-linked glycosylation which occurs at the side chain oxygen of serine (Ser) or threonine (Thr) and (2) N-linked glycosylation which occurs at the side chain nitrogen of an asparagine (Asn) found in the sequence Asn-X-Ser/Thr where X is any amino acid but proline.

The majority of cutinases identified and characterized thus far are of fungal (e.g., FsC, HiC, etc.) and bacterial (e.g., TfC, LCC) origin. Fungi possess an ability to perform both O-linked and N-linked glycosylation of proteins provided the presence of glycosylation sites. FsC, secreted by the phytopathogenic fungus *Fusarium Solano pisi*, was identified as a glycoprotein containing 4.5−5% by weight of carbohydrates (glycans).[40] The glycosylation observed for FsC, produced by its natural host, is O-linked as FsC's sequence lack N-glycosylation site. Several studies have reported cutinase glycosylation when the enzyme was produced by its natural host or by heterologous expression in *Pichia pastoris*/*Saccharomyces cerevisiae*. However, reports on the influence of glycosylation on cutinase expression, catalytic activity and stability are few in number. Recently, our group reported the role of glycosylation on *Thiellavia terrestris* cutinase (TtC) activity and stability.[37,41] For TtC, glycosylation completely inhibited its thermally induced aggregation which, for TtC-NG, is observed at high temperatures.[41] Furthermore, introduction by glycosylation site engineering of one glycosylation site into the fungal cutinase from *Aspergillus oryzae* (AoC, nonglycosylated in nature) resulted in complete inhibition of thermal aggregation and, correspondingly, a 5-fold increase in AoC's kinetic stability at its T_m.[37] In another report,[42] the introduction of an N-Linked glycosylation site in FsC significantly increased enzyme secretion by the heterologous expression systems *S. cerevisiae* or *P. pastoris*.[42] Bacterial cutinases lack glycosylation when expressed by its natural host or heterologously expressed in bacterial cells (e.g., *E. coli*). However, glycosylation can be introduced by introduction of glycosylation site in the protein sequence followed by heterologous expression in eukaryotic expression systems. *N*-linked glycosylation is a preferred choice for engineering due to (i) better control over site specificity and (ii) capability of common eukaryotic expression systems (e.g., *P. pastoris* and *S. cerevisea*) to carry out N-linked glycosylation.

In this study, we interrogate LCC's kinetic stability and subsequent impact it has on PET hydrolysis. We probe global conformational stability through circular dichroism (CD) and fluorescence analysis, aggregation behavior with dynamic light scattering (DLS), and catalytic stability thorough residual activity analysis and temperature optimum screening. In brief we found that LCC tends to aggregate in the native state due to ionic interactions, which can be mitigated with the addition of salt. However, at elevated temperatures, aggregation is driven by perturbation of protein tertiary structure, which is the primary reason for LCC's low kinetic stability. We examined the effects of glycosylation on LCC expressed in *P. pastoris* to address this problem. Glycosylation improved resistance to aggregation even at high temperature conditions leading to a 10 °C increase in the thermal aggregation point and significant increase in kinetic stability. Glycosylation primarily inhibited aggregation and had very little effect on LCC conformational stability. The kinetic stabilization provided by LCC glycosylation was found to have a positive impact on PET hydrolysis activity at high temperatures and enzyme concentrations.

■ MATERIALS AND METHODS

Materials. Salts (Tris, sodium chloride, dibasic and monobasic potassium phosphate) and media components (Luria−Bertani broth [LB], yeast extract, peptone, tryptone, glycerol, and others) and isopropyl β-D-1-thiogalactopyranoside (IPTG) were procured from Sigma. Guanidinium chloride (GdmCl) of molecular biology grade and kanamycin were purchased from Amersham. Zeocine was obtained from Invitrogen. Plasmid vector PET28 and PJ912 were obtained from Genewiz and DNA 2.0, respectively. Amorphous PET films (*lc*PET with crystallinity ~7%) were purchased from Goodfellows USA (ES301445). Bis-hydroxyethyl terephthalate (BHET) and *para*-nitrophenyl butyrate (PNPB) were obtained from Sigma.

Protein Expression and Purification. *Expression and Purification of LCC-NG.* In the context of this study, for clarity, bacterial LCC expressed in *E. coli* is designated as non-glycosylated LCC (LCC-NG). LCC-NG was produced using *E. coli* BL21 DE3 strain by adapting a literature protocol that described the expression of *T. fusca* cutinase.[43] Briefly, The LCC gene codon optimized for *E. coli* expression was cloned in PET28 plasmid vector with kanamycin resistance, which was then transformed into the chemically competent *E. coli* BL21 DE3 cells following a standard transformation protocol published elsewhere.[44] The positive transformants were selected on LB agar plate containing 50 μg/mL kanamycin. The positive transformants were then transferred to fresh culture plates for expression of LCC-NG.

DOI: 10.1021/acs.biochem.7b01189
Biochemistry 2018, 57, 1190−1200

The fermentative production of LCC-NG was performed at a 1 L scale in 2.8 L baffled flasks in the shaker incubator. Seed culture was grown by transforming a single colony of wt-LCC positive *E. coli* strain from fresh agar plate to 100 mL LB medium contain 50 μg/mL kanamycin in a 500 mL flask and incubating at 37 °C and 250 rpm overnight. The production media was composed of terrific broth (12 g/L yeast extract, 24 g/L tryptone, 4.3 g/L KH_2PO_4 and 16 g/L K_2HPO_4) containing 50 μg/mL kanamycin. Production was started by aseptically transferring the seed culture to 1 L of production medium in 2.8 L baffled shake flasks. Cells were grown for 5 h at 37 °C and 250 rpm in the shaker incubator until the cell density reached ~2 absorbance units. Protein expression was then induced by addition of IPTG such that its final concentration is 1 mM. The fermentation was then continued for another 24 h. Bacterial cutinases when expressed in *E. coli*, are transferred (>90%) from the cytoplasm to the culture medium without a need of signal peptide. This phenomenon is attributed to the phospholipid hydrolysis activity of the enzyme which leads to membrane permeation without cell lysis.[45]

At the end of the fermentation, the culture was centrifuged at 5000*g* for 30 min at 4 °C. The resulting cell pellet was discarded whereas the cell free supernatant was subjected to ammonium sulfate precipitation by adding ammonium sulfate to 80% saturation at 25 °C. The precipitate was pelleted down by centrifugation. The precipitate pellet was then solubilized in the loading buffer for affinity purification using a POROS immobilized metal affinity chromatography (IMAC) column. The loading buffer was composed of 20 mM Tris pH 8 with 25 mM imidazole and 200 mM NaCl. Elution was performed using 20 mM Tris pH 8 with 300 mM imidazole and 200 mM NaCl. Guanidinium chloride (GdmCl), final concentration 1 M, was added to the elution fraction followed by concentration by approximately 10-fold using Amicon Ultra 3 kDa centrifugal filters. Subsequently, the protein solution was polished by a size exclusion chromatography (SEC) step. SEC purification was performed using a GE Superose 75 column (23.5 mL). Concentrated protein solution (1 mL) was filtered using a 0.5 μm centrifugal filter and then loaded on to the SEC column with the help of capillary loop. The SEC buffer was composed of 25 mM tris pH 8.0 containing 200 mM sodium chloride and 1 M GdmCl. Purification was carried out at the flow rate of 0.5 mL/min. The purified protein fraction was then extensively dialyzed using 25 mm tris buffer pH 8 containing 200 mM NaCl to remove GdmCl. The resulting protein solution in the same buffer was stored in a refrigerator (5 °C).

Expression and Purification of LCC-G. LCC-G was produced using a *P. pastoris* expression system. The LCC gene was codon optimized and synthesized at DNA2.0 for expression in *P. pastoris*. Integration of the LCC-G gene in *P. pastoris*, subsequent LCC-G fermentative production and purification was performed following published methods used by our group for the heterologous expression of fungal cutinases.[37,41] However, purification of LCC-G required an additional anion exchange chromatography step. The elution pool of the preliminary capture of LCC-G using IMAC chromatography was further purified using a DEAE Sepharose resin in flow through mode. The diethyl amino ethyl (DEAE) Sepharose column was pre-equilibrated with 2 0 mM Tris pH 8 followed by protein loading (up to 30 g/L). A chase step with 20 mM Tris pH 8 buffer containing 100 mM NaCl was used to recover weekly bound protein. Flow through and the chase fractions were pooled together and concentrated ~5−6-times before subsequent dialysis into 20 mM Tris pH 8 buffer. The pure protein was stored in the same buffer in the refrigerator for up to 3−4 weeks. LCC-G variants [N239G, N266Q, and N197Q] were synthesized using identical methods as described above for LCC-G. The LCC-G codon optimized sequence and primers used for LCC-G mutant synthesis by site directed mutagenesis are described in the Supporting Information.

Protein Sample Preparation and Concentration Measurement. Dialysis was used for preparation of protein solutions in desired buffers. Postdialysis, the protein solutions were filtered through 0.5 μm filters. Protein concentration was measured by the standard bicinchonic acid assay (BCA) method with bovine serum albumin (BSA) as the standard followed by dilution to the desired concentration.

Circular Dichroism (CD) Analysis. Circular dichroism was performed using a JASCO J-815 spectropolarimeter coupled with a Peltier-type temperature controller. LCC-G or LCC-NG solutions (10 μM) were prepared in 10 mM Tris pH 8 buffer. CD wavelength scans were performed from 260 to 180 nm wavelength at a scanning rate of 50 nm/min. The CD thermal unfolding scan was performed from 20 to 90 °C at the scan rate of 1 °C/min and the ellipticity at 222 nm was monitored as a function of temperature. The fraction of the unfolded protein was then plotted as a function of temperature where T_m is the temperature at which 50% of the protein is unfolded.

Protein unfolding by GdmCl was determined with 10 μM protein solutions in 10 mM Tris buffer pH 8 containing different concentrations of GdmCl (1 to 6 M). These solutions were freshly prepared by 10× dilution of a 100 μM protein solution in solutions containing predetermined concentrations of GdmCl. Protein-GdmCl solutions were incubated at 25 °C for a sufficient time (48 h) to achieve equilibrium between folded and unfolded states. The protein-GdmCl solutions were then subjected to CD wavelength scans. The average ellipticity from 220 to 224 nm for each GdmCl concentration was recorded. The GdmCl unfolding data was fit to $U = e^f/(1 + e^f)$ where $f = (\Delta G - m[\text{GdmCl}])/RT$ to determine equilibrium free energy of folding in pure water ΔG and m-value.[46] Further, the kinetics of GdmCl unfolding was studied by incubating freshly prepared wt-LCC and LCC-G solutions in 5 M GdmCl (10 μM protein concentrations in pH 8 Tris buffer) at 50 °C in the CD cuvette with constant monitoring of CD ellipticity at 222 nm. The transition in ellipticities at 222 nm as a function of the time was the fitted to eq 1 to determine the apparent rate constant k of unfolding.[11]

$$A(t) - A(\infty) = \sum A\ e^{kt} \tag{1}$$

Fluorescence Analysis. Intrinsic tryptophan fluorescence was measured on a Spex Fluorolog Tau-3 (Horiba) fluorimeter. For protein solutions (2 μM in 10 mM Tris pH 8), excitation was at 295 nm and the emission was recorded from 320 to 350 nM. Slit widths of 2 and 3 nm were used for excitation and emission, respectively. For each wavelength scan of a protein solution, a blank buffer scan was recorded and then subtracted from the corresponding protein scan. The wavelength of the highest fluorescence emission intensity is denoted as the λ_{max}. For thermal transition analyses, the protein solution temperature in the fluorescence measuring cuvette was increased at steps of 5 °C with subsequent 3 min incubations at each temperature. The λ_{max} was then plotted as a function of temperature. The t-T_m (melting point/unfolding temperature for the protein tertiary structure), a measure of protein tertiary structure stability, was determined as the midpoint of the thermal transition.

DOI: 10.1021/acs.biochem.7b01189
Biochemistry 2018, 57, 1190−1200

Dynamic Light Scattering (DLS) Analysis. DLS analyses were performed using a Malvern Zetasizer ZSP90. Thermal scans of 10 μM protein solutions were run from 25 to 90 °C at steps of 5 °C with subsequent 3 min incubations at each temperature. The scattered light intensity was measured as a function of temperature. The onset of aggregation, indicated by an abrupt increase in scattered light intensity, is denoted as the aggregation point (T_{agg}). Furthermore, LCC-G aggregation kinetics was determined by incubation of the protein at both 75 and 80 °C while determining scattered light intensity as a function of time.

Kinetic Stability Analysis. The kinetic stability of LCC-G and LCC-NG at predetermined solution concentration and temperature was determined by measuring the rate of irreversible enzyme activity loss based on PNPB hydrolysis assay.[47] Specifically, 1−10 μM protein solutions in 50 mM HEPES buffer pH 8 was incubated in an Eppendorf thermomixer at varying temperatures (40−95 °C) for 1 h followed by determination of residual activity. The residual activity was then plotted as a function of temperature. $T_{a50/t60}$ (temperature at which enzyme loses 50% of the activity in 60 min) was then noted from the graph as a preliminary measure of the kinetic stability. Based on the $T_{a50/t60}$ values for further evaluation of kinetic stability, the half-life times ($t_{1/2}$) of the enzyme at 70, 75, and 80 °C were determined at predetermined concertation using residual activity analysis at varying time point upon incubation.

PET Hydrolysis Activity Measurement. PET hydrolysis activity was measured using the pH stat based assay previously published by our group.[6] Briefly, *lc*PET films, cut into 0.5 × 0.5 cm^2 pieces, were suspended in 7.5 mL of assay buffer (0.5 mM Tris). The *lc*PET film concentration was varied from 2 to 6 cm^2/mL. Enzyme-film incubations were performed using a Mettler Toledo pH stat to control pH by known quantities of base in response to acid formation (e.g., ester bond hydrolysis). Incubations were magnetically stirred and the temperature was controlled by an external water bath. The substrate solution was first equilibrated for 5 min at the desired reaction temperature and pH. The reaction was then initiated by addition of the enzyme solution at a predetermined concentration (0.015−2 μM). As the reaction progresses, the pH decreases due to cleavage of ester groups that liberate carboxylic acid moieties. The pH stat responds to pH decrease by the automated addition (titration) of dilute sodium hydroxide solution. The enzyme activity was measured as the μmoles of sodium hydroxide added per mL·h of the reaction. The assay was also performed at different temperatures and the reaction rate was plotted as a function of temperature to determine the optimum temperature for enzyme-catalyzed PET hydrolysis.

PET Film Degradation Analysis. *lc*PET film (1 cm × 1 cm) was incubated with 3 mL of 1 μM enzyme solution (LCC-G or LCC-NG) in 500 mM HEPES buffer (pH 8, 70 °C, 100 rpm incubator shaker). At 24 and 48 h of incubation, films were washed extensively with distilled water and dried in a vacuum oven at 50 °C to remove residual moisture. The dried films were then weighed to determine the percent of weight loss.

Bis Hydroxyethyl Terephthalate (BHET) Hydrolysis Activity Analysis. The BHET hydrolysis assay was performed in Eppendorf tubes that contained 100 nM enzyme (LCC-G or LCC-NG) and 0.5 mg/mL BHET (substrate saturation concentration of the 100 nM enzyme solution) in 500 mM HEPES buffer. Eppendorf tubes containing the reaction mixture were placed in an Eppendorf thermomixer that was maintained with agitation (500 rpm) at a predetermined temperature. After 1 h, the reaction was quenched by adding a 2-fold excess of 500 mM pH 2.5 phosphate buffer containing 20% DMSO. The resulting solution was then centrifuged at >20,000*g* for 10 min. Subsequently, HPLC analysis using an Agilent HPLC fit with a Zorbax C-18 column was performed to quantitate formation of terephthalic acid (TA). The mobile phase for HPLC runs consisted of 20% v/v acetonitrile and 0.1% v/v formic acid in Milli-Q water. No-enzyme control experiments were performed for each reaction condition and low level chemical hydrolysis that occurred was subtracted from that due to enzyme-catalyzed hydrolysis. The enzyme activity is given as the millimoles of TA formed per unit time (h) and per milligram of enzyme. Results at different temperatures were used to determine the temperature optimum for the reaction.

■ RESULTS

Expression and Purification of LCC-NG and LCC-G. Transformed *E. coli* BL21 DE3 cells were fermented at a 1 L scale in 2.8 L baffled flasks in a shaker incubator. After cell removal by centrifugation, nonglycosylated wt-LCC (LCC-NG) was purified in three steps that consisted of ammonium sulfate precipitation, immobilized metal affinity chromatography (IMAC) and size exclusion chromatography (SEC). The purified product yield was ∼20 mg/L of the grown culture, where the largest loss in product (50−60%) occurred during SEC. Impurities removed during SEC consisted primarily of high molecular weight LCC-NG aggregates (data not shown). Note that 200 mM NaCl used in IMAC and dialysis buffer is essential to mitigate protein aggregation/precipitation that was observed (even at 4 °C - 25 °C) after solubilization of the ammonium sulfate precipitation pellet. When working with high concentrations (>10 mg/L) of LCC-NG, such as in the SEC equilibration buffer, the strong solubilizing agent 1 M GdmCl was used. In contrast, 200−300 mg/L of glycosylated LCC (LCC-G) was produced by heterologous expression in *P. pastoris* via an optimized protocol we developed for fungal cutinase expression.[47] However, IMAC purified LCC-G had a green color. The extracellular media from the *P. pastoris* cell culture is green colored owing to AOX crystalloid formation;[48] this green color in the case of LCC-G was found to be bind to protein necessitating additional purification. Anion exchange chromatography (AEX) in flow through mode successfully removed the green colored impurity. However, the AEX step resulted in 50−60% yield loss primarily due to removal of LCC-G that was tightly bound to the green impurity. Consequently, pure (green impurity free) LCC-G produced at 110−165 mg/L. Future fermentation optimizations include minimizing production of such green species. Analysis of purified LCC-G by SDS PAGE followed by glycopeptide staining confirmed that LCC was indeed glycosylated (Supporting Information Figure S1). Figure 1 shows the location of the three putative glycosylation sites at N197, N239, and N266 (shown in magenta). Three LCC variants (i) N197Q, N266Q to confirm the presence of glycosylation at N239, (ii) N197Q, N239G to confirm the presence of glycosylation at N266, and (iii) N239G, N266Q to confirm the presence of glycosylation at N197 were designed (see the Supporting Information) and produced in a similar way as that of LCC-G. Indeed, SDS PAGE analysis and glycopeptide staining of these variants confirmed the presence of glycosylation at each of these three sites. (Figure S1).

Circular Dichroism Analysis. CD thermal scans (10 μM protein in 10 mM Tris pH 8 buffer) analyzed the unfolding temperatures of LCC-NG and LCC-G (Figure 2A). The T_m of LCC-NG is 83 °C, which is slightly lower than the reported value

DOI: 10.1021/acs.biochem.7b01189
Biochemistry 2018, 57, 1190−1200

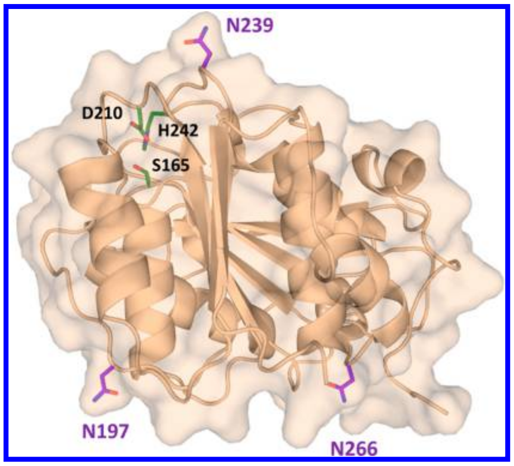

Figure 1. Location of glycosylation sites (shown in magenta) and their relative proximity to LCC's active site (green).

of 86 °C.[11] During the LCC-NG CD thermal scan, visible aggregates appeared in the cuvette, a likely consequence of protein unfolding. In contrast, during the CD thermal scan of LCC-G, no thermal transitions occurred up to the instrument temperature limit (95 °C). Furthermore, during this scan, no visible aggregates were observed in the CD cuvette.

The relative stability of LCC-NG and LCC-G was assessed by comparative GdmCl unfolding. At room temperature, by 36 h, equilibration of LCC-NG and LCC-G unfolding was reached (data not shown). Hence, LCC-NG and LCC-G were incubated at different GdmCl concentrations for 48 h before CD analysis of secondary structure. LCC-G showed marginally higher stability against GdmCl unfolding (Figure 2B and Table 1). Further, LCC-G also had higher stability at 50 °C in the presence of 5 M GdmCl. That is, LCC-G undergoes thermal unfolding approximately two times slower than LCC-NG (see Figure 3). Table 1 lists the kinetics constants for both LCC-NG and LCC-G unfolding.

Fluorescence Analysis. Intrinsic tryptophan fluorescence emission monitors changes in protein tertiary structure as a function of a perturbation such as temperature. When buried, tryptophan residues generally display emission maxima (λ_{max})

Table 1. Thermodynamic and Kinetic Constants for LCC-NG and LCC-G Calculated from the Equilibrium GdmCl Unfolding and Unfolding Kinetics Analysis

protein	C_m (M)	m (kJ mol^{-1} M^{-1})	ΔG (kJ mol^{-1})	$\Delta\Delta G$ (kJ mol^{-1})	K_i* (min^{-1})
LCC-NG	3.8	−6.0	22.6	0	0.0012
LCC-G	4.1	−6.4	26.0	−3.4	0.025

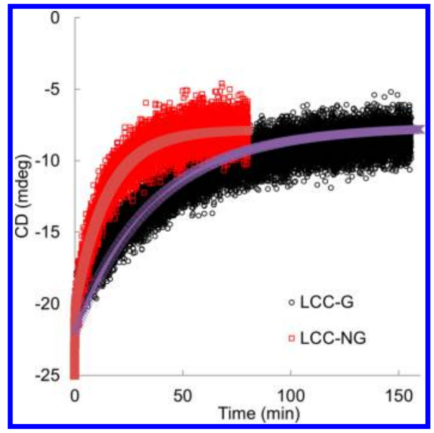

Figure 3. Effect of glycosylation on the unfolding kinetics of LCC-NG and LCC-G (10 μm protein concentration, 5 M GdmCl in 10 mM Tris pH 8 at 50 °C).

around 330 nm; which shifts to longer wavelength (>340 nm) upon solvent exposure. Thus, a λ_{max} shift with increased temperature indicates a change in local tryptophan environment.[49] Fluorescence analysis (Figure 4) of thermal unfolding for LCC-NG and LCC-G protein solutions (2 μM in 10 mM Tris pH 8) reveals that the thermal stability of LCC-G is slightly higher (t-T_m of 77 and 75 °C for LCC-G and LCC-NG, respectively). In contrast to the CD thermal scan (up to 95 °C), LCC-NG aggregation was not visually observed in the cuvette. This difference is attributed to the lower protein concentration (2 μM vs 10 μM) used for fluorescence analysis.

Aggregation Analysis. Scattered light intensity was monitored as it passed through a DLS cuvette to gain further insights on LCC-G and LCC-NG thermal induced aggregation.

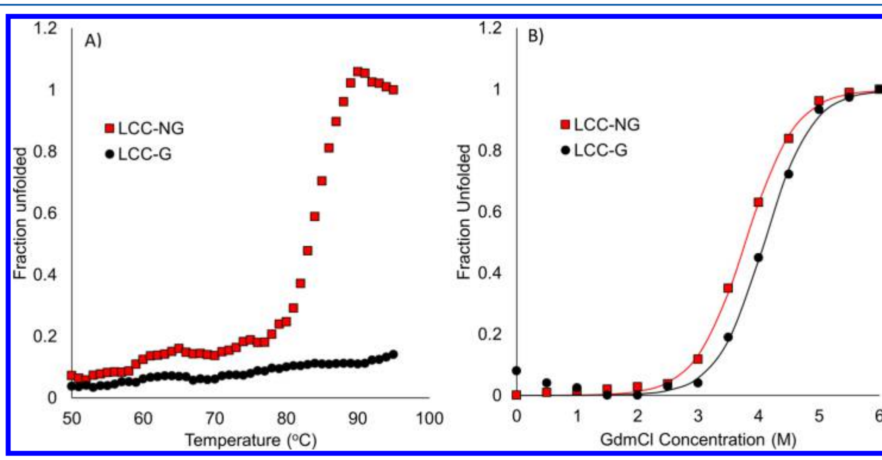

Figure 2. CD analysis of (a) thermal-induced unfolding and (b) GdmCl-induced unfolding (continuous lines indicate fitted data). Studies were performed for LCC-NG and LCC-G at 10 μM protein concentrations in 10 mM tris buffer pH 8).

DOI: 10.1021/acs.biochem.7b01189
Biochemistry 2018, 57, 1190−1200

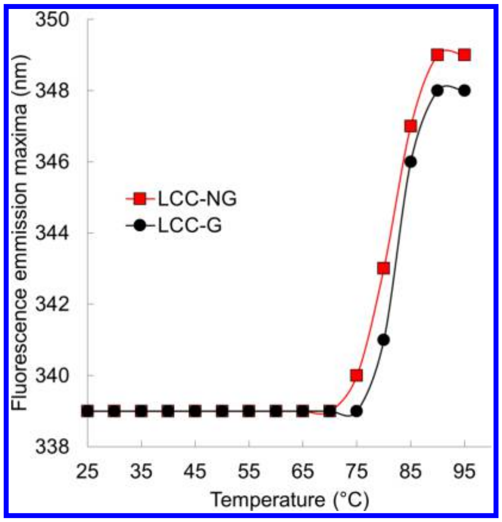

Figure 4. Fluorescence analysis temperature scans to identify thermal-induced unfolding of LCC-NG and LCC-G (2 μM protein in 10 mM tris buffer pH 8).

Plots of scattered light intensity as a function of temperature as well as time at fixed temperatures are displayed in Figure 5A and B, respectively. Inspection of Figure 5A shows scattered light increases at the aggregation temperatures (T_{agg}) of 80 and 70 °C for LCC-G and LCC-NG, respectively. The magnitude of change in light scattering at T_{agg} is much greater for LCC-NG. These results are consistent with the observation that visible aggregates form and eventually settle to the bottom of the cuvette for LCC-NG but not LCC-G during CD thermal scans up to 95 °C. Subsequently, scattered light intensity was used to study the effect of incubation time on LCC-G aggregation at 75 and 80 °C (Figure 5B). At both temperatures, an increase in light intensity is observed with increased incubation time confirming that LCC-G also forms aggregates. Relative to 75 °C, incubation at 80 °C results in a more rapid increase in scattered light. Nevertheless, aggregates formed by LCC-G are not observed visually indicating they are likely at the nanoscale and/or involve a small population of the protein molecules.

Kinetic Stability Analysis. Residual activity is a measure of irreversible enzyme activity loss. When measured as a function of time, residual activity measurements provide insights into inactivation kinetics. Residual activity measurements for 1 μM solutions (50 mM HEPES buffer, pH 8) of LCC-G and LCC-NG after 60 min incubations were performed at different temperatures. Both LCC-NG and LCC-G showed good kinetic stability, retaining >85% activity at temperatures up to 75 °C for one h. However, at 80 °C, LCC-G and LCC-NG retained 85% and 50% activity, respectively (Figure 6). Furthermore, at 85 °C, LCC-G and LCC-NG retained 10% and no activity, respectively.

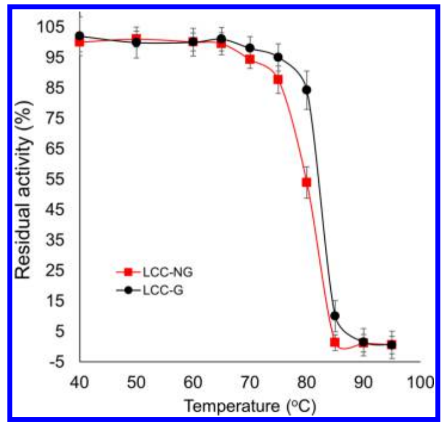

Figure 6. Residual activity analysis of LCC-NG and LCC-G (1 μM protein in 50 mM HEPES buffer pH 8) upon incubation for an hour at predetermined temperatures.

We further determined the $t_{1/2}$ of 1 μM LCC-NG and LCC-G solutions (50 mM HEPES buffer, pH 8) at 70 °C, 75 °C, and 80 °C (Table 2). Both LCC-NG and LCC-G have high stabilities at 70 and 75 °C. However, at 80 °C, LCC-G is 3 times more stable than its nonglycosylated counterpart. For both LCC-G and LCC-NG, increase in their concentrations from 1 to 10 μM at 70 °C resulted in substantial decreases in $t_{1/2}$ values (Table 2).

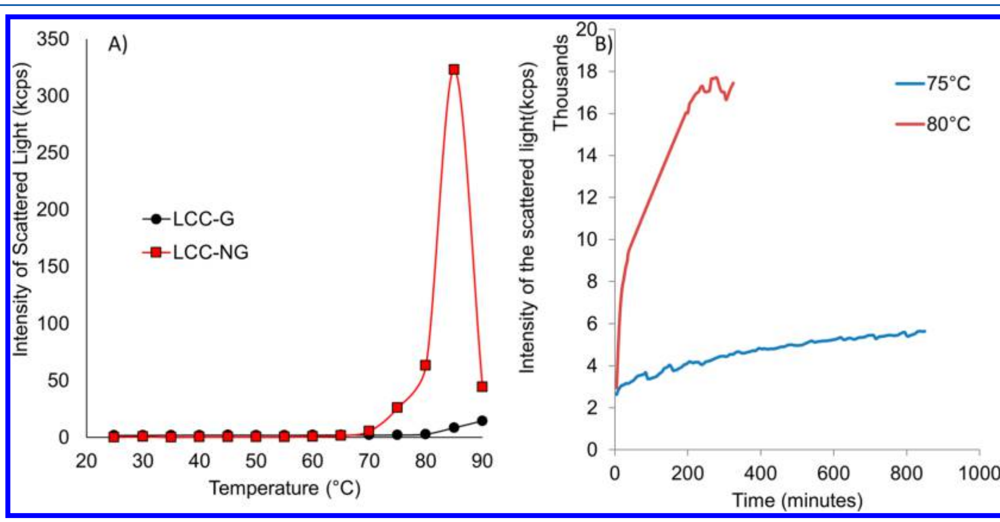

Figure 5. DLS analysis of LCC-G and LCC-NG (10 μM protein in 10 mM tris buffer pH 8): (a) thermal-induced aggregation analysis and (b) kinetics of the thermal-induced aggregation of LCC-G at 75 and 80 °C.

DOI: 10.1021/acs.biochem.7b01189
Biochemistry 2018, 57, 1190−1200

Table 2. Kinetic Stability of LCC-NG and LCC-G to Determine Half-Life Time ($t_{1/2}$) Values at 70, 75, and 80 °C

		$t_{1/2}$ (h)	
T (°C)	enzyme concn (μM)	LCC-NG	LCC-G
70	1	~51	~60
75	1	~35	~50
80	1	1.1	3.2
70	10	~24	~35

Nevertheless, under these latter conditions, $t_{1/2}$ for LCC-G is ~1.5-times greater than that for LCC-NG.

Temperature Optimum for the Enzyme Activity. Measurement of the optimal PET hydrolysis temperatures for both LCC-NG and LCC-G was by pH stat (Figure 7). The temperature optimum for both LCC-NG and LCC-G was 75 °C on *lc*PET (Figure 7B). However, at higher temperatures (from 65 to 80 °C), LCC-G had significantly higher activity. Indeed, at 70 and 75 °C, LCC-G was 1.6- and 1.2-fold more active, respectively (Figure 7A).

The solid-state properties of PET change as one approaches the glass transition temperature, T_g (about 70 °C). To better isolate the extent that solid-state transitions have on the observed differences between LCC-NG and LCC-G, we measured activity on the water-soluble substrate bis-hydroxyethyl terephthalate (BHET) (Figure 7B). The temperature−activity profiles for both LCC-NG and LCC-G on BHET showed: (i) identical activity over the full temperature range and (ii) a temperature optimum of 50 °C.

PET Hydrolysis Kinetics. Since enzymatic hydrolysis of PET requires that the enzyme adsorb from the aqueous medium to the substrate, we adopted a kinetic model developed by Scandola and co-workers that accounts for enzyme−substrate heterogeneity.[50] Activity was measured at 70 °C (as a compromise between the optimal temperatures for enzyme activity and kinetic stability) with increasing enzyme concentrations over constant substrate concentration. For LCC-NG, *lc*PET hydrolysis activity increased with increasing enzyme concentration until a plateau was reached at 0.5 μM (Figure 8). The plateau is attributed to enzyme saturation of substrate surfaces. Further increase in LCC-NG concertation resulted in decreased activity. In contrast, LCC-G hydrolysis of *lc*PET as a function of enzyme concentration reveals a conventional heterogeneous kinetics profile in which *lc*PET hydrolysis activity plateaued at 0.5 μM LCC-G and remained constant with further increase in the enzyme concentration. Activities of LCC-NG and LCC-G are similar up to 0.25 μM enzyme concentration. However, above 0.25 μM, LCC-G showed significantly higher *lc*PET hydrolysis activity (Figure 8).

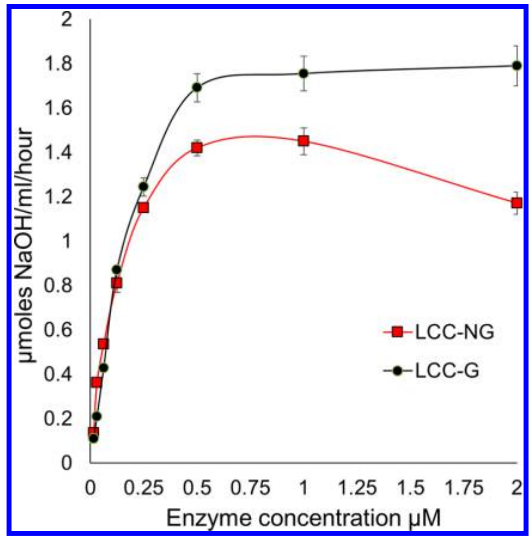

Figure 8. PET hydrolysis activity of LCC-NG and LCC-G at predetermined enzyme concentrations (70 °C in 5 mM tris buffer, pH 8 and 2 cm^2/mL substrate concentration).

PET Film Degradation Analysis. Both LCC-NG and LCC-G showed very good PET hydrolysis activity with complete degradation of 1 cm^2 *lc*PET film (1 cm x 1 cm and 250 μm thick) in 3 mL of 1 μM enzyme solution (70 °C, pH 8). After 24 and 48 h of incubation, both LCC-NG and LCC catalyzed the formation of water-soluble products such that PET films underwent about

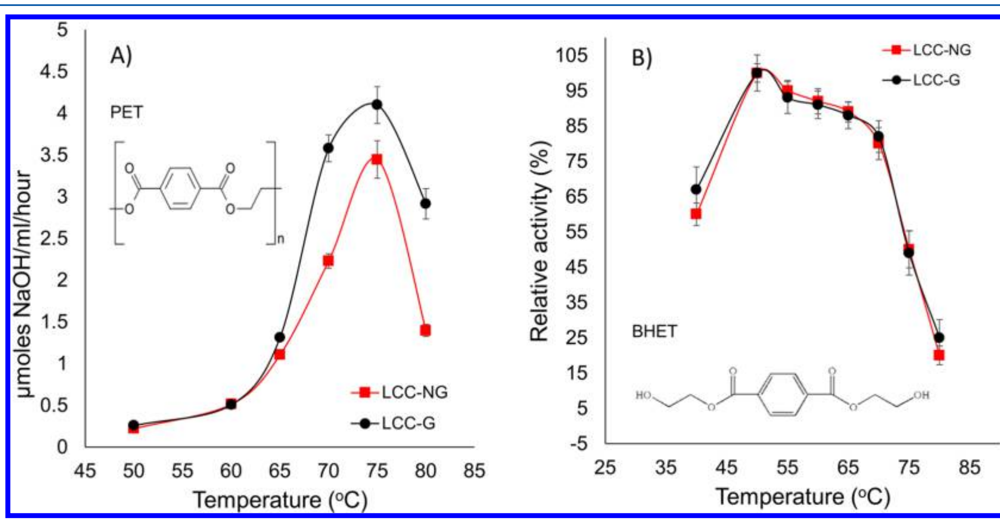

Figure 7. Influence of temperature on LCC-NG and LCC-G activity for (a) PET hydrolysis measures using a pH stat (1 μM enzyme in 5 mM tris buffer, pH 8 and 6 cm^2/mL substrate concentration) and (b) bis-hydroxyethyl terephthalate (BHET) hydrolysis (100 nM enzyme in 500 mM HEPES buffer pH 8 with 0.5 mg/mL BHET).

DOI: 10.1021/acs.biochem.7b01189
Biochemistry 2018, 57, 1190−1200

25% and nearly complete ~95% weight loss, respectively. Taking thickness of *lc*PET films (250 μM) into account complete weight loss in 48 h represents degradation rate of 60 μm per day (per film side) with an enzyme coverage of 0.085 per square centimeter.

■ DISCUSSION

Effect of Glycosylation on the Conformational Stability of LCC. *Global Conformational Stability.* CD thermal unfolding scans of LCC-NG and LCC-G (Figure 2A) demonstrate that glycosylation markedly improves LCC thermostability. Although the T_m for LCC-G could not be determined due to instrument limitations, the lack of an unfolding transition up to 95 °C indicates that LCC-G's T_m is more than 12 °C above that of LCC-NG. However, the extent of LCC stabilization mediated by glycosylation reported here is significantly higher than previous reports for other enzymes, e.g., cutinases,[37] phytases,[35,51] peroxidases,[52,53] lipases,[54] *etc.,* which indicate up to 1 °C - 4 °C increases in T_m by glyosylation. Increases in T_m by glycosylation have been attributed to (i) *enthalpic stabilization*, in which the native state is stabilized by interactions of glycans with surrounding amino acids (e.g hydrogen bonding),[55] and (ii) *entropic stabilization*, where the glycosylated proteins native state is entropically favored.[33]

We measured stability in the presence of GdmCl to probe the mechanism of LCC stabilization by glycosylation. Surprisingly, glycosylation only conferred modest improvements against GdmCl denaturation (Figure 2B). Thermostabilization often correlates with stability against GdmCl unfolding;[56] hence, the large deference between stabilization by glycosylation against thermal and GdmCl unfolding seems anomalous or hints that thermal and GdmCl unfolding of LCC have significantly different mechanisms, requiring more detailed investigation (vide infra). Further, we probed the effect of LCC glycosylation on thermostability and tertiary structure by intrinsic tryptophan fluorescence analysis. Unlike thermal unfolding monitored by CD, a clear thermal-induced transition was observed for both variants, with LCC-G having a marginally higher unfolding temperature (Figure 4). These observations are consistent with the modest thermodynamic stabilization provided by glycosylation against GdmCl-mediated unfolding. However, the fluorescence thermal scan indicates that LCC-NG's tertiary structure unfolding temperature (t-T_m) is ~8 °C lower than the CD thermal scan measured T_m (75 °C vs 83 °C). Similarly, LCC-*G*'s tertiary structure unfolding temperature (t-T_m) measured by a fluorescence thermal scan is 77 °C whereas the CD T_m is >95 °C. These observations are consistent with a unfolding mechanism where loss of tertiary structure begins at the fluorescence determined unfolding temperature. This partial loss of tertiary structure exposes hydrophobic side chains that can contribute to aggregation. It then follows that LCC-NG aggregation, observed visually in the CD cuvette, results in tertiary structure loss as observed by CD. In contrast, LCC-G did not show visible thermal aggregation even above t-T_m (77 °C).

CD thermal scans were performed in the presence of 2 M GdmCl to eliminate effects of thermal aggregation in LCC-G vs LCC-NG secondary structure stability comparisons (Figure S2). GdmCl provided a 2-fold advantage: (i) inhibition of LCC-NG thermal-induced aggregation and (ii) the denaturation activity of GdmCl brought the thermal transition of LCC-G within the temperature limit of the CD instrument. Under these conditions, glycosylation was found to have only a modest (2 °C) stabilizing effect on the secondary structure, which is consistent with the effect of glycosylation on tertiary structure stability (t-T_m) as measured by fluorescence. However, glycosylation did have a large effect on thermal unfolding kinetics, which occurs two-times slower for LCC-G (see Figure 3 and Table 1). These observations imply that glycosylation provides significant secondary structure kinetic stabilization.

Active Site Stability. Loss of enzyme activity can arise from disruptions to the global conformation or local active site structure. While unfolding experiments provide insights into the global conformational stability, the optimum enzyme activity temperature is a measure of active site stability. Previously, Sulaiman et al. reported a large gap (~36 °C) between LCC-NG active site and global stability (T_{opt}= 50 °C and T_m = 86 °C, respectively). One of the three LCC glycosylation sites (N239) is close to the active site (9 Å to D210, Figure 1), which may stabilize the structure of neighboring enzyme regions. The optimum temperature of LCC-NG for BHET hydrolysis is consistent with that reported by Sulaiman et al. and glycosylation was not found to stabilize the active site for BHET hydrolysis (Figure 7A). However, solution phase (homogeneous catalysis) temperature−activity profiles observed here are different than that reported by Sulaiman et al., who observed a sharp optimum at 50 °C for PNPB hydrolysis. That is, while we found the BHET hydrolysis optimum for LCC-NG and LCC-G is also at 50 °C, activity for both LCC-NG and LCC-G gradually decreases with increasing temperature to 70 °C, where ~80−85% of LCC's activity is retained. Generally, both T_{opt} values for PNPB and BHET hydrolysis activities would be considered good indicators of active site stability. However, the differences in PNPB and BHET temperature−activity profiles indicate that binding of the latter stabilizes the active site.

BHET docked to the active site of LCC shows potential aromatic stacking interactions between the substrate and F243 which may contribute to the stabilizing effect of BHET (Figure S3). Moreover, mere binding of polymeric chains near the active site can provide a stabilizing effect. Sulaiman et al. have reported LCC-NG active-site stabilization by polyethylene glycol (PEG) and hypothesized that PEG binding near the active site imparts local stability, which was supported by computational modeling.[11]

Stabilization against Thermal Aggregation. LCC-NG's high propensity for aggregation is evident by its precipitation from solution during various stages of purification, even at 4−25 °C. However, precipitation is mitigated by addition of 0.1 to 1 M NaCl (depending upon the protein concentration) in purification buffers. Salt inhibition of aggregation indicates that ionic interactions contribute to aggregation events. Indeed, LCC presents a highly charged surface, with several positively and negatively charged patches (Figure S4). In contrast, glycosylation of LCC resulted in a large decrease in its propensity to aggregate, which may be due to steric constraints that inhibit charge−charge interactions.

Thermal aggregation analysis revealed that LCC-NG has a high propensity for aggregation above 70 °C (Figure 5A). This is attributed to partial disruption of LCC-NG's tertiary structure that enhances hydrophobic interactions. Further evidence that LC-NG thermal-induced aggregation is driven by hydrophobic interactions is that, addition of up to 1 M salt did not influence LCC-NG aggregation at 70 °C (data not shown).

The T_{agg} for LCC-G is 10 °C above that of LCC-NG (Figure 5A). Furthermore, LCC-G T_{agg} is ~5 °C higher than the onset temperature of tertiary structure loss measured by fluorescence analysis (~75 °C, Figure 4). Thus, for LCC-G, aggregation is

DOI: 10.1021/acs.biochem.7b01189
Biochemistry 2018, 57, 1190−1200

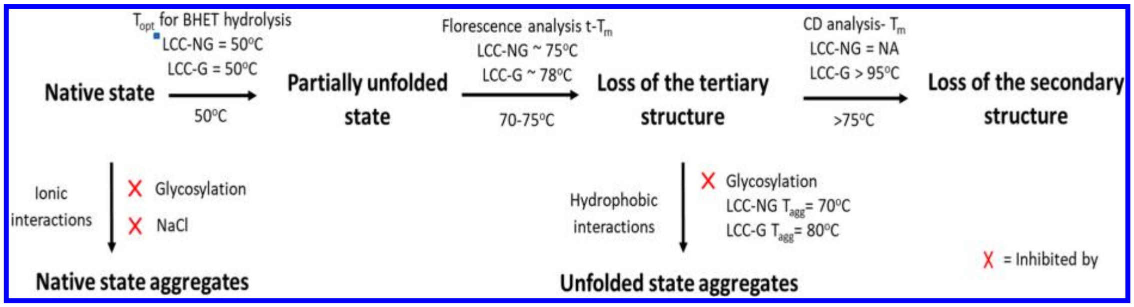

Figure 9. Schematic of LCC-NG and LCC-G thermal inactivation.

inhibited after partial tertiary structure loss. Inhibition of irreversible aggregation by glycosylation shifts the equilibrium between native and unfolded states toward the native state, resulting in protein kinetic stabilization.[35,37] Indeed, this stabilization against thermal aggregation results in increased kinetic stability at higher temperatures and enzyme concentrations (Table 1). These observations are consistent with our previous reports of AoC stabilization by glycosylation.[37] However, for AoC, the introduction of a single glycosylation at a rationally selected site results in full aggregation inhibition. In contrast, LCC-G has three glycosylation sites and shows the formation of soluble aggregates (albeit at 10 °C higher than its nonglycosylated counterpart). Since LCC's three glycosylation sites are fixed by its native sequence, glycosylation site engineering may be an avenue for further improvements.

DLS thermal scans were recorded for designed LCC-G variants glycosylated at only one location to determine individual contributions of each glycosylation site to the 10 °C improvement in T_{agg}, (see Supporting Information Figure S5). We found that glycosylation at N266 and N197 primarily contributes to the stabilization against thermal aggregation whereas glycosylation at N239 had only a negligible effect. Interestingly, glycosylation at either N266 or N197 is sufficient to provide stabilization against thermal aggregation. These observations, taken together with our previous report on AoC stabilization, indicate that a single glycosylation site, especially one well positioned, can provide robust stabilization against thermal-induced aggregation. Although stabilized by glycosylation, the aggregation observed with LCC-G at or above its T_{agg} like LCC-NG can be attributed to partial disruption of LCC-NG's tertiary structure that enhances hydrophobic interactions.

Inactivation Pathway for LCC-G and LCC-NG. Based on CD, fluorescence, and T_{opt} analysis, an inactivation mechanism for LCC-NG and LCC-G inactivation mechanism is proposed in Figure 9. Both variants display a similar thermal inactivation pathway where LCC-G has higher stability due to glycosylation that provides conformational and colloidal stabilization. In summary, LCC-NG exhibits native state aggregation, attributed to ionic interactions. However, native state LCC aggregation may be mitigated by salt or by glycosylation. Thermal inactivation of both LCC-NG and LCC-G follows local unfolding (based on T_{opt}) which is then followed by loss of tertiary structure (based on t-T_m) and then secondary structure (based on CD T_m). Glycosylation was found to moderately stabilize the thermal transition of both tertiary and the secondary structure of LCC (based on fluorescence and CD thermal scans). However, glycosylation does not have any effect on active site stabilization. Further the major stabilizing effect of glycosylation is visible at higher temperature where the rapid aggregation induced by the conformational changes of LCC-NG is substantially mitigated in case of LCC-G (based on thermal aggregation analysis). LCC-G dsisplays 10 °C higher aggregation point as compared to its nonglycosylated counterpart.

Effect of the Glycosylation on the Catalytic Performance. An important metric that will influence the effectiveness of an enzyme for PET biocatalytic recycling is stability at or above PET's T_g (70 °C). Sulaiman et al. reported that, at 70 °C, the $t_{1/2}$ of 2 μM LCC-NG is 40 min.[5] In contrast, results reported show that, at 70 °C, the $t_{1/2}$ of LCC-NG is ~52 and 24 h at 1 μM and 10 μM concentrations, respectively. Note that we used 50 mM HEPES buffer pH 8 for this study (to ensure pH stability at higher temperature) where Sulaiman et al. used 50 mM Tris pH 8 (pH is <8 at 70 °C for the same buffer). For further comparison, we adopted the buffer conditions used by Sulaiman et al. At 70 °C under these conditions we find that LCC-NG has significantly higher kinetic stability ($t_{1/2}$ = 40 h) than that reported by Sulaiman et al. ($t_{1/2}$ = 40 min). The reasons for the lower kinetic stability of LCC-NG reported by Sulaiman et al. are unclear.

LCC, which has 3 putative N-glycosylation sites, was expressed in *P. pastoris* to further improve LCC's kinetic stability. The resulting glycosylated protein, LCC-G, has higher kinetic stability than LCC-NG (~1.5-times at 75 °C and about 3-fold at 80 °C, see Table 2). This improvement in LCC's kinetic stability enhances LCC's PET hydrolysis activity. Indeed, comparative analysis of PET hydrolysis activity by LCC-G and LCC-NG at 70 °C, 75 and 80 °C showed that LCC-G has significantly higher activity (Figure 7A). Furthermore, at concentrations above 0.25 μM, the *lc*PET hydrolysis activity of LCC-G is significantly higher than LCC-NG (Figure 8). Indeed, this decrease in LCC-NG activity at concentrations above 0.25 μM is due to thermal-induced aggregation that increases in propensity at relatively higher concentrations. For LCC-G, thermal-induced aggregation at 70 °C in this concentration range is largely inhibited by glycosylation. A long-term *lc*PET film degradation study at 70 °C (500 mM HEPES, pH 8) with LCC-NG and LCC-G both resulted in ~25% and ~95% weight loss at 24 and 48 h, respectively. The retention of LCC-NG enzyme activity during this long-term study may be due to the high buffer concentration (500 mM) that negates potential pH decreases due to release of acid moieties of terephthalic acid. Indeed LCC-NG aggregation is inhibited at high salt concentration. Further studies will be needed to better understand the relative performance of LCC-G and LCC-NG performance for PET hydrolysis under realistic process conditions.

■ CONCLUSIONS

Wt-LCC (LCC-NG) displays high global conformational stability based on T_m values determined by CD and fluorescence

DOI: 10.1021/acs.biochem.7b01189
Biochemistry 2018, 57, 1190−1200

thermal scans (83 and 75 °C, respectively). However, LCC-NG is highly prone to aggregation. Indeed, electrostatic interactions resulted in its precipitation even at room temperature and low concentrations (10−20 μM). Hence, the purification and storage of LCC-NG requires use of salts at concentrations that vary with protein concentration. Further, efficient PET hydrolysis requires LCC-NG to be active at or above 70 °C, which is very close to the onset tertiary structure loss. At this temperature, LCC undergoes rapid aggregation which is a function of its concentration. This behavior imposes limitations on its practical applications such as for catalysis of PET hydrolysis.

LCC's bacterial origin results in its nonglycosylated native state. However, biosynthesis of glycosylated LCC inhibits LCC thermal-induced aggregation. Consequently, glycosylated LCC (LCC-G) enables facile purification and high concentration storage without salt. Further, the onset of thermal induced aggregation temperature for LCC-G is 10 °C higher than LCC-NG. Moreover, the rate of aggregation for LCC-G was found to be slow compared to the rapid aggregation of LCC-NG at or above 70 °C. Stabilization of LCC by glycosylation also enables an improvement in the catalytic performance of LCC for PET hydrolysis. That is, LCC-G is significantly more active than LCC-NG at higher temperature (above 65 °C) while retaining activity at higher concentrations relative to its nonglycosylated counterpart. Hence, glycosylation of LCC is a powerful stabilization strategy that can be applied to other aggregation prone proteins regardless of their bacterial origin.

■ ASSOCIATED CONTENT

Supporting Information

The Supporting Information is available free of charge on the ACS Publications website at DOI: 10.1021/acs.biochem.7b01189.

> LCC protein sequence, nucleotide sequence, primers for LCC glycosylation site variants; confirming LCC glycosylation by SDS PAGE analysis; CD thermal-induced unfolding scan of LCC-NG and LCC-G in the presence of 2 M GdmCl; BHET docked to the active site of LCC: potential aromatic stacking interactions between the substrate and F243; calculated electrostatic surface potential of LCC; comparative thermal aggregation of LCC-NG, LCC-G, and LCC_G glycosylation site variants (PDF)

■ AUTHOR INFORMATION

Corresponding Author

*Phone: 518-276-3734. Fax: 518-276-3405. E-mail: grossr@rpi.edu.

ORCID

Allison Zwarycz: 0000-0001-6830-5765
Robert J. Linhardt: 0000-0003-2219-5833
Richard A. Gross: 0000-0002-5050-3162

Funding

This work was supported by the National Science Foundation Award # 1067415 to R.A.G.

Notes

The authors declare no competing financial interest.

■ ACKNOWLEDGMENTS

We thank Professor Romas J. Kazlauskas for his revision and suggestions towards constructing this manuscript.

■ REFERENCES

(1) Wei, R., and Zimmermann, W. (2017) Microbial enzymes for the recycling of recalcitrant petroleum-based plastics: how far are we? *Microb. Biotechnol. 10* (6), 1308−1322.

(2) Wei, R., and Zimmermann, W. (2017) Biocatalysis as a green route for recycling the recalcitrant plastic polyethylene terephthalate. *Microb. Biotechnol. 10* (6), 1302−1307.

(3) Yoshida, S., Hiraga, K., Takehana, T., Taniguchi, I., Yamaji, H., Maeda, Y., Toyohara, K., Miyamoto, K., Kimura, Y., and Oda, K. (2016) A bacterium that degrades and assimilates poly(ethylene terephthalate). *Science (Washington, DC, U. S.) 351*, 1196−1199.

(4) Ferrario, V., Pellis, A., Cespugli, M., Guebitz, G., and Gardossi, L. (2016) Nature Inspired Solutions for Polymers: Will Cutinase Enzymes Make Polyesters and Polyamides Greener? *Catalysts 6*, 205.

(5) Sulaiman, S., Yamato, S., Kanaya, E., Kim, J.-J., Koga, Y., Takano, K., and Kanaya, S. (2012) Isolation of a novel cutinase homolog with polyethylene terephthalate-degrading activity from leaf-branch compost by using a metagenomic approach. *Appl. Environ. Microbiol. 78*, 1556−62.

(6) Ronkvist, Å. M., Xie, W., Lu, W., and Gross, R. a. (2009) Cutinase-Catalyzed Hydrolysis of Poly(ethylene terephthalate). *Macromolecules 42*, 5128−5138.

(7) Vertommen, M. a M. E., Nierstrasz, V. a, Van Der Veer, M., and Warmoeskerken, M. M. C. G. (2005) Enzymatic surface modification of poly(ethylene terephthalate). *J. Biotechnol. 120*, 376−86.

(8) Maiti, I. B., Kolattukudy, P. E., and Shaykh, M. (1979) Purification and characterization of novel cutinase from nasturtium (Tropaeolum majus) pollen. *Arch. Biochem. Biophys. 196*, 412−423.

(9) Nielsen, A. D., Borch, K., and Westh, P. (2007) Thermal stability of Humicola insolens cutinase in aqueous SDS. *J. Phys. Chem. B 111*, 2941−7.

(10) Chen, S., Tong, X., Woodard, R. W., Du, G., Wu, J., and Chen, J. (2008) Identification and characterization of bacterial cutinase. *J. Biol. Chem. 283*, 25854−62.

(11) Sulaiman, S., You, D.-J., Kanaya, E., Koga, Y., and Kanaya, S. (2014) Crystal structure and thermodynamic and kinetic stability of metagenome-derived LC-cutinase. *Biochemistry 53*, 1858−69.

(12) Nicoud, L., Owczarz, M., Arosio, P., and Morbidelli, M. (2015) A multiscale view of therapeutic protein aggregation: A colloid science perspective. *Biotechnol. J. 10*, 367−378.

(13) Amin, S., Barnett, G. V., Pathak, J. A., Roberts, C. J., and Sarangapani, P. S. (2014) Protein aggregation, particle formation, characterization & rheology. *Curr. Opin. Colloid Interface Sci. 19*, 438−449.

(14) Buell, A. K., Hung, P., Salvatella, X., Welland, M. E., Dobson, C. M., and Knowles, T. P. J. (2013) Electrostatic Effects in Filamentous Protein Aggregation. *Biophys. J. 104*, 1116−1126.

(15) Majhi, P. R., Ganta, R. R., Vanam, R. P., Seyrek, E., Giger, K., and Dubin, P. L. (2006) Electrostatically Driven Protein Aggregation: β-Lactoglobulin at Low Ionic Strength. *Langmuir 22*, 9150−9159.

(16) Jiang, L., Cao, S., Cheung, P. P.-H., Zheng, X., Leung, C. W. T., Peng, Q., Shuai, Z., Tang, B. Z., Yao, S., and Huang, X. (2017) Real-time monitoring of hydrophobic aggregation reveals a critical role of cooperativity in hydrophobic effect. *Nat. Commun. 8*, 15639.

(17) Münch, C., and Bertolotti, A. (2010) Exposure of Hydrophobic Surfaces Initiates Aggregation of Diverse ALS-Causing Superoxide Dismutase-1 Mutants. *J. Mol. Biol. 399*, 512−525.

(18) Lebendiker, M., and Danieli, T. (2014) Production of prone-to-aggregate proteins. *FEBS Lett. 588*, 236−246.

(19) Rosa, M., Roberts, C. J., and Rodrigues, M. A. (2017) Connecting high-temperature and low-temperature protein stability and aggregation. *PLoS One 12*, e0176748.

(20) Vaezzadeh, M., Sabbaghian, M., Yaghmaei, P., and Ebrahim-Habibi, A. (2017) Effect of Organic Solvents on Porcine Pancreatic Lipase Thermal Aggregation. *Protein Pept. Lett. 24*, 955−961.

(21) Pfefferkorn, C. M., McGlinchey, R. P., and Lee, J. C. (2010) Effects of pH on aggregation kinetics of the repeat domain of a functional amyloid, Pmel17. *Proc. Natl. Acad. Sci. U. S. A. 107*, 21447−21452.

(22) Mleko, S., and Foegeding, E. A. (2000) pH Induced Aggregation and Weak Gel Formation of Whey Protein Polymers. *J. Food Sci. 65*, 139−143.

(23) Colombié, S., Gaunand, A., Rinaudo, M., and Lindet, B. (2000) Irreversible lysozyme inactivation and aggregation induced by stirring: kinetic study and aggregates characterisation. *Biotechnol. Lett. 22*, 277−283.

(24) Kamal, M. Z., Ahmad, S., Molugu, T. R., Vijayalakshmi, A., Deshmukh, M. V., Sankaranarayanan, R., and Rao, N. M. (2011) In Vitro Evolved Non-Aggregating and Thermostable Lipase: Structural and Thermodynamic Investigation. *J. Mol. Biol. 413*, 726−741.

(25) O'Brien, C. J., Blanco, M. A., Costanzo, J. A., Enterline, M., Fernandez, E. J., Robinson, A. S., and Roberts, C. J. (2016) Modulating non-native aggregation and electrostatic protein−protein interactions with computationally designed single-point mutations. *Protein Eng., Des. Sel. 29*, 231−243.

(26) Matsui, D., Nakano, S., Dadashipour, M., and Asano, Y. (2017) Rational identification of aggregation hotspots based on secondary structure and amino acid hydrophobicity. *Sci. Rep. 7*, 9558.

(27) Arakawa, T., and Timasheff, S. N. (1985) The stabilization of proteins by osmolytes. *Biophys. J. 47*, 411−4.

(28) Arakawa, T., and Timasheff, S. N. (1982) Stabilization of protein structure by sugars. *Biochemistry 21*, 6536−6544.

(29) Kolate, A., Baradia, D., Patil, S., Vhora, I., Kore, G., and Misra, A. (2014) PEG — A versatile conjugating ligand for drugs and drug delivery systems. *J. Controlled Release 192*, 67−81.

(30) Moreno-Pérez, S., Orrego, A. H., Romero-Fernández, M., Trobo-Maseda, L., Martins-DeOliveira, S., Munilla, R., Fernández-Lorente, G., and Guisan, J. M. (2016) Intense PEGylation of Enzyme Surfaces. *Methods Enzymol. 571*, 55−72.

(31) Hey, T., Knoller, H., and Vorstheim, P. (2012) Half-Life Extension through HESylation, in *Therapeutic Proteins*, pp 117−140, Wiley-VCH Verlag GmbH & Co. KGaA, Weinheim, Germany.

(32) Winterburn, P. J., and Phelps, C. F. (1972) The Significance of Glycosylated Proteins. *Nature 236*, 147−151.

(33) Shental-Bechor, D., and Levy, Y. (2008) Effect of glycosylation on protein folding: a close look at thermodynamic stabilization. *Proc. Natl. Acad. Sci. U. S. A. 105*, 8256−61.

(34) DeKoster, G. T., and Robertson, A. D. (1997) Thermodynamics of unfolding for Kazal-type serine protease inhibitors: entropic stabilization of ovomucoid first domain by glycosylation. *Biochemistry 36*, 2323−31.

(35) Høiberg-Nielsen, R., Fuglsang, C. C., Arleth, L., and Westh, P. (2006) Interrelationships of Glycosylation and Aggregation Kinetics for *Peniophora lycii* Phytase †. *Biochemistry 45*, 5057−5066.

(36) Høiberg-Nielsen, R., Westh, P., Skov, L. K., and Arleth, L. (2009) Interrelationship of steric stabilization and self-crowding of a glycosylated protein. *Biophys. J. 97*, 1445−1453.

(37) Shirke, A. N., Su, A., Jones, J. A., Butterfoss, G. L., Koffas, M. A. G., Kim, J. R., and Gross, R. A. (2017) Comparative thermal inactivation analysis of *Aspergillus oryzae* and *Thiellavia terrestris* cutinase: Role of glycosylation. *Biotechnol. Bioeng. 114*, 63−73.

(38) Wang, C., Eufemi, M., Turano, C., and Giartosio, a. (1996) Influence of the carbohydrate moiety on the stability of glycoproteins. *Biochemistry 35*, 7299−7307.

(39) Shental-Bechor, D., and Levy, Y. (2009) Folding of glycoproteins: toward understanding the biophysics of the glycosylation code. *Curr. Opin. Struct. Biol. 19*, 524−533.

(40) Lin, T.-S., and Kolattukudy, P. E. (1980) Structural Studies on Cutinase, a Glycoprotein Containing Novel Amino Acids and Glucuronic Acid Amide at the N Terminus. *Eur. J. Biochem. 106*, 341−351.

(41) Shirke, A. N., Basore, D., Holton, S., Su, A., Baugh, E., Butterfoss, G. L., Makhatadze, G., Bystroff, C., and Gross, R. A. (2016) Influence of surface charge, binding site residues and glycosylation on Thielavia terrestris cutinase biochemical characteristics. *Appl. Microbiol. Biotechnol. 100*, 4435−4446.

(42) Sagt, C. M. J., Kleizen, B., Verwaal, R., De Jong, M. D. M., Muller, W. H., Smits, A., Visser, C., Boonstra, J., Verkleij, A. J., and Verrips, C. T. (2000) Introduction of an N-glycosylation site increases secretion of heterologous proteins in yeasts. *Appl. Environ. Microbiol. 66*, 4940−4944.

(43) Su, L., Hong, R., and Wu, J. (2015) Enhanced extracellular expression of gene-optimized Thermobifida fusca cutinase in Escherichia coli by optimization of induction strategy. *Process Biochem. 50*, 1039−1046.

(44) Chung, C. T., Niemela, S. L., and Miller, R. H. (1989) One-step preparation of competent Escherichia coli: transformation and storage of bacterial cells in the same solution. *Proc. Natl. Acad. Sci. U. S. A. 86*, 2172−2175.

(45) Su, L., Woodard, R. W., Chen, J., and Wu, J. (2013) Extracellular Location of Thermobifida fusca Cutinase Expressed in Escherichia coli BL21(DE3) without Mediation of a Signal Peptide. *Appl. Environ. Microbiol. 79*, 4192−4198.

(46) Myers, J. K., Pace, C. N., and Scholtz, J. M. (1995) Denaturant m values and heat capacity changes: relation to changes in accessible surface areas of protein unfolding. *Protein Sci. 4*, 2138−2148.

(47) Shirke, A. N., Basore, D., Butterfoss, G. L., Bonneau, R., Bystroff, C., and Gross, R. A. (2016) Toward rational thermostabilization of Aspergillus oryzae cutinase: Insights into catalytic and structural stability. *Proteins: Struct., Funct., Genet. 84*, 60−72.

(48) Ozimek, P., Veenhuis, M., and Vanderklei, I. (2005) Alcohol oxidase: A complex peroxisomal, oligomeric flavoprotein. *FEMS Yeast Res. 5*, 975−983.

(49) Stryer, L. (1968) Fluorescence spectroscopy of proteins. *Science 162*, 526−533.

(50) Scandola, M., Focarete, M. L., and Frisoni, G. (1998) Simple kinetic model for the heterogeneous enzymatic hydrolysis of natural poly (3-hydroxybutyrate). *Macromolecules 31*, 3846−3851.

(51) Guo, M., Hang, H., Zhu, T., Zhuang, Y., Chu, J., and Zhang, S. (2008) Effect of glycosylation on biochemical characterization of recombinant phytase expressed in *Pichia pastoris*. *Enzyme Microb. Technol. 42*, 340−345.

(52) Tams, J. W., and Welinder, K. G. (1998) Glycosylation and thermodynamic versus kinetic stability of horseradish peroxidase. *FEBS Lett. 421*, 234−236.

(53) Tams, J. W., and Welinder, K. G. (2001) Kinetic Stability of Designed Glycosylation Mutants of Coprinus cinereus Peroxidase. *Biochem. Biophys. Res. Commun. 286*, 701−706.

(54) Zhu, J., Liu, H., Zhang, J., Wang, P., Liu, S., Liu, G., and Wu, L. (2014) Effects of Asn-33 glycosylation on the thermostability of Thermomyces lanuginosus lipase. *J. Appl. Microbiol. 117*, 151−159.

(55) Barb, A. W., Borgert, A. J., Liu, M., Barany, G., and Live, D. (2010) Intramolecular Glycan−Protein Interactions in Glycoproteins. *Methods Enzymol. 478*, 365−388.

(56) Wang, Q., Christiansen, A., Samiotakis, A., Wittung-Stafshede, P., and Cheung, M. S. (2011) Comparison of chemical and thermal protein denaturation by combination of computational and experimental approaches. II. *J. Chem. Phys. 135*, 175102.

DOI: 10.1021/acs.biochem.7b01189
Biochemistry 2018, 57, 1190−1200